



# Denoising using deep-learning-based reconstruction for whole-heart coronary MRA with sub-millimeter isotropic resolution at 3 T: a volunteer study

Toshiya Kariyasu   
Haruhiko Machida   
Sanae Takahashi   
Keita Fukushima   
Tatsuya Yoshioka   
Kenichi Yokoyama 

## PURPOSE

The aim of this study was to assess the usefulness of denoising deep-learning-based reconstruction (dDLR) to improve image quality and vessel delineation in noncontrast 3-T whole-heart coronary magnetic resonance angiography (WHCMRA) with sub-millimeter isotropic resolution (Sub-mm) compared with a standard resolution without dDLR (Standard).

## METHODS

For 10 healthy volunteers, we acquired the WHCMRA with Sub-mm with and without dDLR and Standard to quantify signal- (SNR) and contrast-to-noise ratio (CNR) and vessel edge signal response (VESR) in all the 3 image types. Two independent readers subjectively graded vessel sharpness and signal homogeneity of 8 coronary segments in each patient. We used Kruskal-Wallis test with Bonferroni correction to compare SNR, CNR, VESR, and the subjective evaluation scores among the 3 image types and weighted kappa test to evaluate inter-reader agreement on the scores.

## RESULTS

SNR was significantly higher with Sub-mm with dDLR ( $P < .001$ ) and Standard ( $P = .005$ ) than with Sub-mm without dDLR and was comparable between Sub-mm with dDLR and Standard ( $P = .511$ ). CNR was significantly higher with Sub-mm with dDLR ( $P < .001$ ) and Standard ( $P = .005$ ) than with Sub-mm without dDLR and was comparable between Sub-mm with dDLR and Standard ( $P = .560$ ). VESR was significantly greater with Sub-mm with ( $P = .001$ ) and without dDLR ( $P = .017$ ) than with Standard and was comparable between Sub-mm with and without dDLR ( $P = 1.000$ ). In the proximal, middle, distal, and all the coronary segments, the subjective vessel sharpness was significantly better with Sub-mm with dDLR than Sub-mm without dDLR and Standard ( $P < .001$ , for all) and was comparable between Sub-mm without dDLR and Standard ( $P > .05$ ); the subjective signal homogeneity was significantly improved from Sub-mm without dDLR to Standard to Sub-mm with dDLR ( $P < .001$ ). The inter-reader agreement was excellent ( $\kappa = 0.84$ ).

## CONCLUSION

Application of dDLR is useful for improving image quality and vessel delineation in the WHCMRA with Sub-mm compared with Standard.

Three-dimensional (3D) whole-heart coronary magnetic resonance angiography (WHCMRA) is a noninvasive imaging method for assessing coronary artery stenosis and is advantageous over coronary computed tomography angiography (CCTA) because it does not require radiation exposure or contrast media administration and is only slightly susceptible to calcium-related artifacts.<sup>1-3</sup> Because WHCMRA is commonly limited in delineation of distal coronary segments and quantification of vessel lumen stenosis due to its insufficient spatial resolution and anisotropy, some investigators have used various techniques to acquire WHCMRA with sub-millimeter isotropic resolution (Sub-mm) whose image quality is not necessarily satisfactory at 1.5 T, within an acceptable acquisition time.<sup>4-6</sup> While a steady-state free precession (SSFP) sequence has been commonly applied in noncontrast WHCMRA at 1.5 T, increased B1 field inhomogeneity, frequency offset from tissue susceptibility variation, and specific absorption rate limit consistency of SSFP at 3 T. As such, the spoiled gradient-echo sequence, which decreases the signal-to-noise ratio (SNR) of the coronary arteries, has often been used at 3 T.<sup>7-10</sup>

From the Department of Radiology (T.K., H.M.,  
✉ hmachida@ks.kyorin-u.ac.jp, K.Y.), Faculty of  
Medicine, Kyorin University, Tokyo, Japan (T.K., H.M.),  
Tokyo Women's Medical University Adachi Medical  
Center, Adachi-ku, Tokyo, Japan and (S.T., K.F., T.Y.),  
Kyorin University Hospital, Tokyo, Japan.

Received 30 April 2021; revision requested 27 May  
2021; last revision received 13 September 2021;  
accepted 31 October 2021.

Publication date: 15 August 2022.

DOI: 10.5152/dir.2022.21291

You may cite this article as: Kariyasu T, Machida H, Takahashi S, Fukushima K, Yoshioka T, Yokoyama K. Denoising using deep-learning-based reconstruction for whole-heart coronary MRA with sub-millimeter isotropic resolution at 3 T: A volunteer study. *Diagn Interv Radiol.* 2022;28(5):470-477.

**Table 1.** Acquisition and reconstruction parameters

	Sub-mm w/ dDLR	Sub-mm w/o dDLR	Standard
Matrix size	336 × 336		192 × 272
In-plane resolution	0.9 × 0.9 mm <sup>2</sup>		1.6 × 1.1 mm <sup>2</sup>
Slice thickness	0.9 mm		1.5 mm
Number of slices	120		72
TR		5 ms	
TE		1.9 ms	
Flip angle		12°	
Bandwidth		326 Hz/pixel	
FOV		30 × 30 cm <sup>2</sup>	
Acceleration factor		2	
Fast 3D mode (k-sampling ratio)	Wheel (80%)		Off (100%)
Acquisition time	7 : 47 ± 0 : 46 min		3 : 37 ± 0 : 30 min
Reconstructed voxel size	0.45 × 0.45 × 0.45 mm <sup>3</sup>		0.8 × 0.55 × 0.75 mm <sup>3</sup>
dDLR	On		Off

Sub-mm, sub-millimeter isotropic resolution; dDLR, a denoising method with deep-learning-based reconstruction; Standard, a standard resolution without dDLR; TR, repetition time; TE, echo time; FOV, field of view.

A 3-T clinical MR scanner with a maximum gradient magnetic field of 100 mT/m (the slew rate: 200 mT/m/ms) has been recently introduced and can offer thinner slice images at the same bandwidth (i.e., the same sampling interval/time). With this scanner, a denoising method with deep-learning-based reconstruction (dDLR) has been newly developed using a convolution neural network (CNN) to improve SNR in high-resolution MR images without additional scan time.<sup>11</sup> Currently, this dDLR algorithm (Advanced intelligent Clear-IQ Engine [AiCE], Canon Medical Systems Corporation) is clinically available only from the single vendor. While some smoothing filters frequently applied in clinical settings

### Main points

- A denoising method with deep-learning-based reconstruction (dDLR) uses a deep convolution neural network to reduce image noise in magnetic resonance images without additional scan time.
- dDLR can be applied to improve signal-(SNR) and contrast-noise ratio in noncontrast 3-T whole-heart coronary magnetic resonance angiography (WHCMRA) using a spoiled gradient-echo sequence, which offers lower SNR than a steady-state free precession sequence commonly applied at 1.5 T.
- Combined application of dDLR and sub-millimeter isotropic resolution is useful for improving vessel sharpness, signal homogeneity, and delineation of the coronary arteries in the WHCMRA.

are designed to reduce high-frequency noise at the cost of image blurring, we hypothesized that dDLR should only reduce image noise without any negative influence on the delineation of the coronary vessels in WHCMRA. Thus, we performed volunteer studies to assess usefulness of dDLR to improve image quality and coronary vessel delineation in noncontrast WHCMRA with Sub-mm compared with a standard resolution without dDLR (Standard) using this 3-T scanner.

## Methods

### Subjects

The present study was approved by the institutional review board (approval number: 620), and informed consent was obtained from each volunteer. Ten healthy volunteers (10 men; mean age, 40.9 ± 12.4

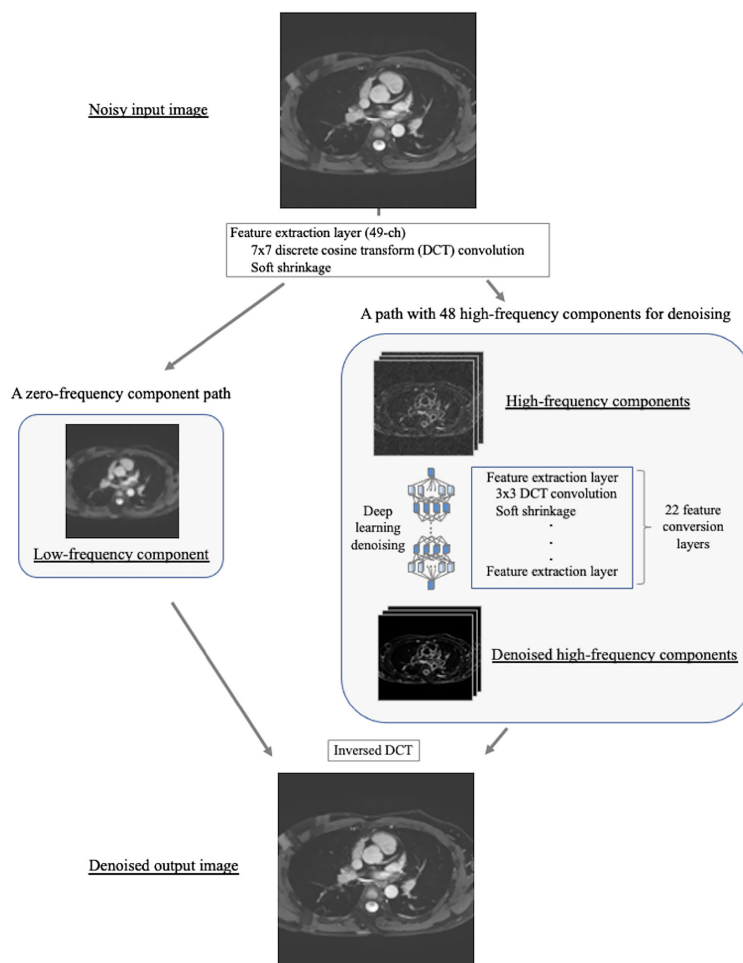


**Figure 1.** Schematic diagram of the dDLR processing. First, the noisy input image is divided into the 0-frequency component and the other 48 high-frequency components with a fixed 7 × 7 DCT basis. Next, the 48 high-frequency components go through denoising path, and the 0-frequency component is bypassed. The denoising path consists of multiple convolution layers with an activation function. Finally, all the components are transformed into a denoised output image. DCT, discrete cosine transform; dDLR, deep-learning-based reconstruction.

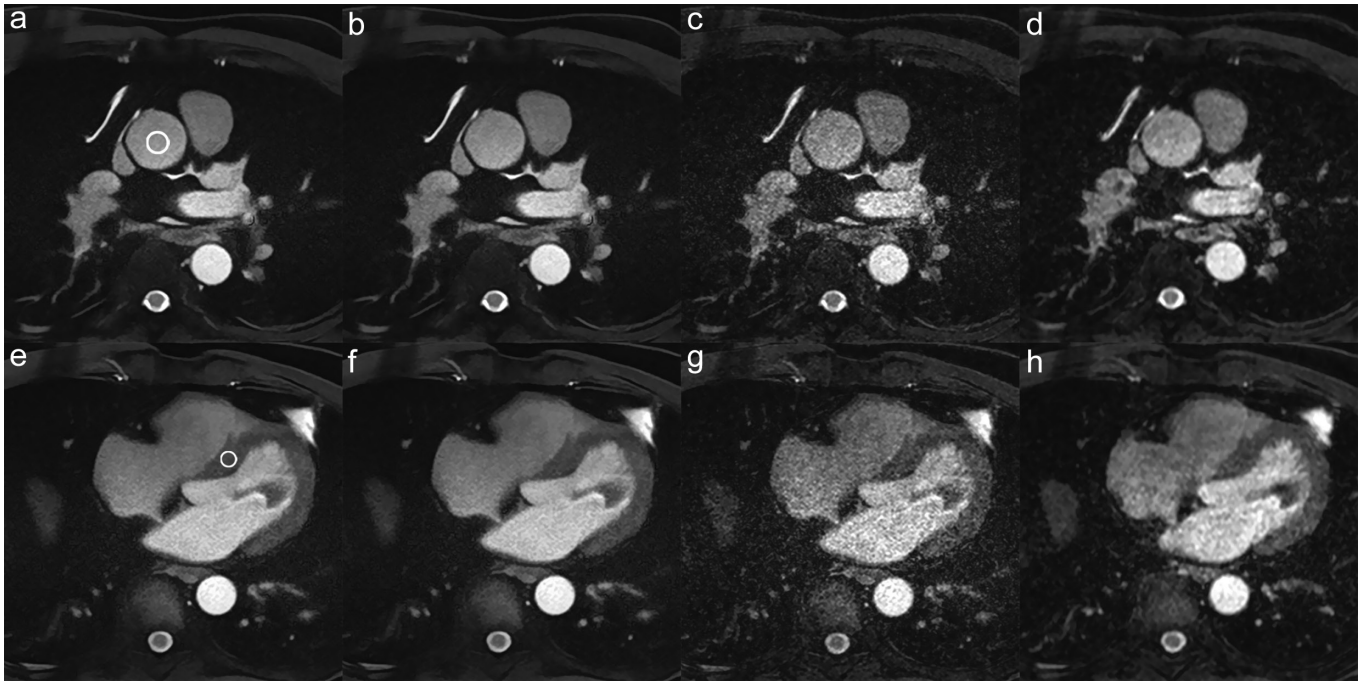


**Figure 2.** Axial images of WHCMRA for a 57-year-old man with Sub-mm w/ (a, b, e, f) and w/o dDLR (c, g) and Standard (d, h) at the levels of the root of the ascending aorta (a-d) and the interventricular septum (e-h). Circular ROIs are placed in the root of the ascending aorta (a) and the interventricular septum (e) to quantify SNR and CNR as shown in this WHCMRA with Sub-mm w/ dDLR. Both SNR and CNR decreased from Sub-mm w/ dDLR (SNR, 40.0; CNR, 27.7) (b, f) to Standard (SNR, 37.9; CNR, 26.1) (d, h) to Sub-mm w/o dDLR (SNR, 17.5; CNR, 12.0) (c, g), as represented by subjective image noise increasing in this order. SNR, signal-to-noise ratio; CNR, contrast-to-noise ratio; WHCMRA, whole-heart coronary magnetic resonance angiography; ROI, region of interest.

years; range, 26-57 years; mean body mass index,  $23.8 \pm 2.2$  kg/m<sup>2</sup>, range, 22.6-27.2 kg/m<sup>2</sup>; mean heart rate,  $66.7 \pm 12.9$  bpm, range, 44-90 bpm) were recruited for the present study. All the subjects had no prior medical problems, such as cardiac diseases

or respiratory diseases, that would interfere with the examinations. No  $\beta$ -blocker or nitroglycerine was administered to any of the subjects.

### Image acquisition

All these volunteers underwent non-contrast 3D WHCMRA with a 3-T clinical MR scanner with a highest gradient magnetic field of 100 mT/m (Vantage Galan 3T/ZGO, Canon) equipped with 16-channel phased-array body and spine coils (Atlas SPEEDER Body & Spine Coil, Canon) using a respiration motion correction (Real-time Motion Correction, Canon), electrocardiography-triggered 3D-spoiled gradient-echo sequence (T1WI fast field echo 3D, Canon) with the spectral attenuated inversion recovery (SPAIR) method for fat suppression. The order of applied pulses was as follows: inversion pulse for SPAIR, T2 preparation pulse, the respiration motion correction pulse, and dummy pulse. Here, we time-efficiently applied the T2 preparation pulse, the respiration motion correction pulse, and the dummy pulse during waiting time for the null point of the longitudinal magnetization of fat signal in SPAIR technique without elongating acquisition time. The matrix size was  $336 \times 336$  for Sub-mm and  $192 \times 272$  for Standard; the in-plane resolution was  $0.9 \times 0.9$  mm<sup>2</sup> and  $1.6 \times 1.1$  mm<sup>2</sup>; slice thickness was 0.9 mm and 1.5 mm; the number of slices was 120 and 72. Other scan parameters were the same for both resolutions: repetition time,

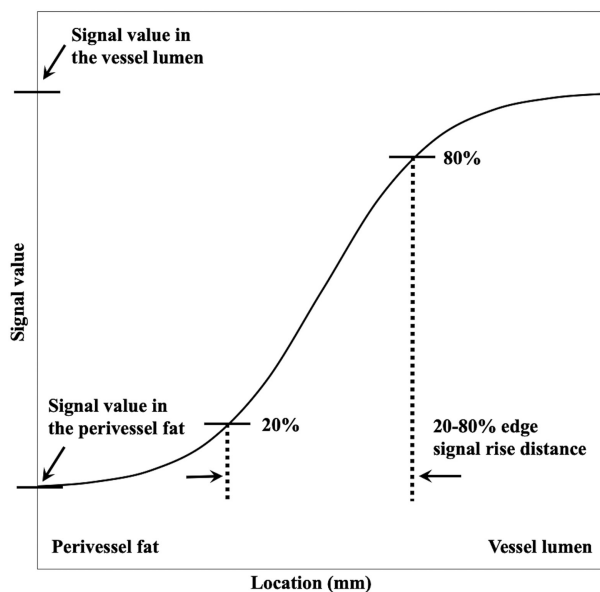


**Figure 3.** Graph illustrating definition of  $ESRD_{20\%-80\%}$ . Graph shows signal value in relation to pixel location along a profile curve drawn from fat surrounding the coronary vessel to the vessel lumen over the vessel edge.  $ESRD_{20\%-80\%}$ , 20%-80% edge signal rise distance, is defined as distance for pixel signal value to rise from 20% to 80% of difference between signal values in the perivessel fat and the vessel lumen. Shorter  $ESRD_{20\%-80\%}$  represents sharper edge.

5 ms; echo time, 1.9 ms; flip angle, 12°; bandwidth, 326 Hz/pixel; field of view, 30 × 30 cm<sup>2</sup>. Parallel imaging (SPEEDER, Canon) was applied in the phase-encoding direction with an acceleration factor of 2. Only for Sub-mm, we employed a novel k-space filling technique for fast image acquisition, a “wheel” technique (k-sampling ratio: 80%) in Fast 3D mode (Canon) for acquiring signals at the center of the k-space in a deformed wheel pattern in the phase encode (y-axis)-slice encode (z-axis) plane. These acquisition parameters are summarized in Table 1.

### Image reconstruction

Image reconstruction was completed within a couple of minutes in each WHCMRA examination even with Sub-mm with dDLR (w/ dDLR). Two radiology technologists with 11-year experience reconstructed WHCMRA axial images with a slice thickness of 0.9 mm (i.e., reconstructed voxel size: 0.45 × 0.45 × 0.45 mm<sup>3</sup>) w/ dDLR and without dDLR (w/o dDLR) for Sub-mm and 1.5 mm (i.e., reconstructed voxel size: 0.8 × 0.55 × 0.75 mm<sup>3</sup>) for Standard and used these images to reconstruct curved multiplanar reformation images of the 3 major coronary vessels: right coronary artery (RCA), left anterior descending artery (LAD), and left circumflex artery (LCX) (Table 1).

The dDLR method used in this study was a denoising technique based on deep CNN (DCNN). The technique is currently commercially available as AiCE for clinical

use in WHCMRA<sup>12</sup> as well as in MR imaging of other regions, such as brain, urinary bladder, and women’s pelvis.<sup>11-16</sup> The algorithm has been described in detail in the previous study.<sup>11</sup> Figure 1 illustrates an outline of the dDLR algorithm. The algorithm divides the noisy input image data into the 0-frequency component and the remaining high-frequency components. Specifically, a 7 × 7 discrete cosine transform (DCT) convolution is used to separate one 0-frequency component and the other 48 high-frequency components in the dDLR algorithm.<sup>11</sup> One 0-frequency basis of the 7 × 7 DCT convolution is used to generate the 0-frequency component, and the other 48 bases are used to generate the 48 high-frequency components. Next, the high-frequency components go through denoising path which consists of multiple convolution layers to reduce noise, and the 0-frequency component is bypassed. Finally, all the components are transformed into a denoised output image. Separation of this zero-frequency component from the denoising path enables to preserve the image contrast.

This technique requires 2 steps: training and inference. The training step is a process of building the DCNN model using a lot of pairs of high SNR images and low SNR images. The inference step is the process of removing noise using the built model. In this study, the same trained model was used as in the previous study.<sup>11</sup> Specifically, a total of 32 400 image patch pairs were

generated from 8 head and knee MR images (the maximal spatial resolution: 0.22 mm) using T1, T2, T2\*, and proton density-weighted and fluid-attenuated inversion recovery protocols. All images were acquired 10 times at the same slice position with the 3-T MR scanner. The high SNR target images were generated by rigid image registration followed by averaging of the 10 acquired images.

### Quantitative image quality assessment

The radiology technologists placed 4 regions of interest in both the root of the ascending aorta and the interventricular septum to measure the mean value and standard deviation (SD) of their signal intensities in WHCMRA axial images of Sub-mm w/ and w/o dDLR and Standard in each subject using a copy-and-paste function (Figure 2). The background noise was defined as the mean SD of the signal intensity in the interventricular septum; SNR, the mean signal intensity in the ascending aorta divided by the background noise; and CNR, the difference of the mean signal intensity between the ascending aorta and interventricular septum divided by the background noise. We calculated the mean values of the SNR and CNR in all the subjects.

One of the radiology technologists drew a profile curve on the cross-section of proximal RCA and left main trunk (LMT) to proximal LAD as proximal left coronary artery (LCA) in WHCMRA of Sub-mm w/

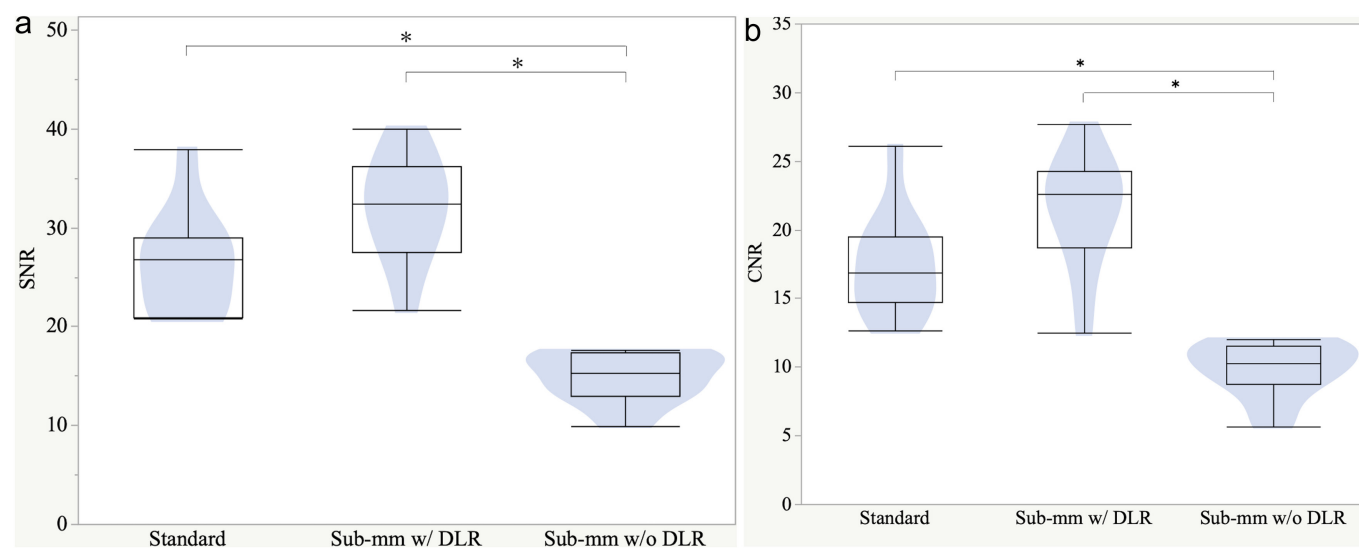


**Figure 4.** Violin plots with box-and-whisker plots representing SNR (a) and CNR (b) in WHCMRA with Sub-mm w/ and w/o dDLR and Standard. SNR (a) is significantly higher with Sub-mm w/ dDLR ( $P < .001$ ) and Standard ( $P = .005$ ) than with Sub-mm w/o dDLR and was comparable between Sub-mm w/ dDLR and Standard ( $P = .511$ ). CNR (b) is significantly higher with Sub-mm w/ dDLR ( $P < .001$ ) and Standard ( $P = .005$ ) than with Sub-mm w/o dDLR and was comparable between Sub-mm w/ dDLR and Standard ( $P = .560$ ). The asterisks represent statistical significance ( $P < .05$ ). SNR, signal-to-noise ratio; CNR, contrast-to-noise ratio; WHCMRA, whole-heart coronary magnetic resonance angiography.

and w/o dDLR and Standard in each subject. We assessed sharpness of the coronary vessel edge to quantify edge response as the distance for edge signal rise of 20%-80% (ESRD<sub>20%-80%</sub>), distance for pixel signal value to rise from 20% to 80% of difference between signal values in fat surrounding the vessel and the vessel lumen, for the both proximal coronary arteries in the 3 imaging types in each subject (Figure 3).<sup>17</sup> Here, shorter ESRD<sub>20%-80%</sub> represents sharper edge.

### Qualitative image quality assessment

All the WHCMRA images were randomly arranged and reviewed on a workstation (Ziostation2, Ziosoft, Inc). Based on coronary segments, visual evaluation scores regarding sharpness and signal homogeneity of the major coronary vessels were independently graded by a board-certified radiologist with 13-year experience (reader 1) and the one of the radiology technologists with 11-year experience (reader 2) who

were blinded to the types of the images. The coronary segments were defined according to the American Heart Association 15-segment model as follows: #1, proximal RCA; #2, middle RCA; #3, distal RCA; #5, LMT; #6, proximal LAD; #7, middle LAD; #8, distal LAD; #11, proximal LCX; and #13, distal LCX. #4AV was used as an alternative to #13 in 3 subjects where distribution of the coronary artery showed RCA-dominant pattern. Segments #1, #5-6, and #11 were defined as proximal; segments #2 and #7 as middle; and #3, #8, and #13 (or #4AV) as distal. The sharpness of the vessels was graded based on a 4-point scale with respect to their border definition as follows: 1, severely blurred and uninterpretable; 2, moderately blurred but interpretable; 3, mildly blurred; and 4, sharply defined. The signal homogeneity of the vessels was graded as follows: 1, very inhomogeneous and uninterpretable; 2, inhomogeneous but interpretable; 3, almost homogeneous; and 4, completely homogeneous.

### Statistical analysis

All continuous variables were expressed as mean  $\pm$  SD. We analyzed statistics using commercially available software (IBM SPSS Statistics, version 27 IBM SPSS). We used Wilcoxon signed-rank test to compare the mean acquisition time between Sub-mm and Standard. Kruskal-Wallis test with Bonferroni correction was used to compare the SNR, CNR, ESRD<sub>20%-80%</sub> for the both proximal coronary arteries, and the visual evaluation scores in the proximal, middle, distal, and all coronary segments among Sub-mm w/ and w/o dDLR and Standard. Weighted kappa ( $\kappa$ ) test was used to evaluate the inter-reader agreement on the visual evaluation scores. Values of  $\kappa$  were interpreted as follows: poor, 0.00-0.20; fair, 0.21-0.40; moderate, 0.41-0.60; good, 0.61-0.80; and excellent, 0.81-1.00. Here, *P*-values lower than .05 were considered statistically significant.

## Results

The mean acquisition time was significantly longer with Sub-mm (7 : 47  $\pm$  0 : 46 min) than with Standard (3 : 37  $\pm$  0 : 30 min) (*P* = .005), as shown in Table 1. The SNR was significantly higher with Sub-mm w/ dDLR (29.1  $\pm$  10.9) (*P* < .001) and Standard (24.6  $\pm$  9.2) (*P* = .005) than with Sub-mm w/o dDLR (13.3  $\pm$  5.0) and was comparable between Sub-mm w/ dDLR and Standard (*P* = .511) (Figures 2 and 4a). The CNR was

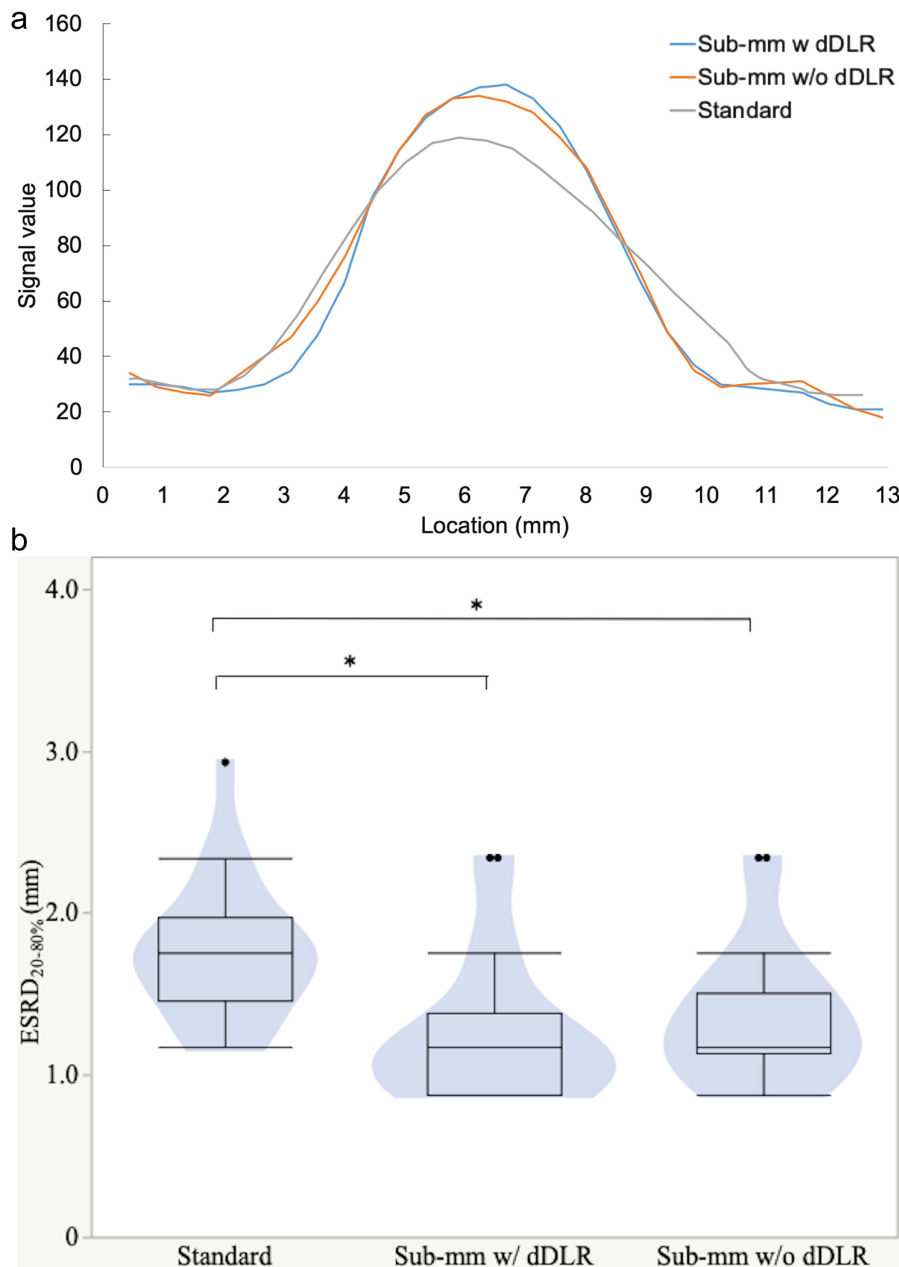


**Figure 5.** Representative profile curves on the cross-section of the proximal coronary artery (a) and violin plots with box-and-whisker plots representing ESRD<sub>20%-80%</sub> (b) in WHCMRA with Sub-mm w/ and w/o dDLR and Standard. The both slopes of the profile curves (a) are steeper with Sub-mm w/ and w/o dDLR than with Standard and are comparable between Sub-mm w/ and w/o dDLR. ESRD<sub>20%-80%</sub> (b) is significantly shorter with Sub-mm w/ (*P* = .001) and w/o dDLR (*P* = .017) than with Standard and is comparable between Sub-mm w/ and w/o dDLR (*P* = 1.000). The asterisks represent statistical significance (*P* < .05). ESRD<sub>20%-80%</sub> distance for edge signal rise of 20%-80%.

significantly higher with Sub-mm w/ dDLR ( $19.5 \pm 7.5$ ) ( $P < .001$ ) and Standard ( $16.1 \pm 6.3$ ) ( $P = .005$ ) than with Sub-mm w/o dDLR ( $8.9 \pm 3.4$ ) and was comparable between Sub-mm w/ dDLR and Standard ( $P = .560$ ) (Figures 2 and 4b). ESRD<sub>20%-80%</sub> for proximal RCA and LCA was significantly shorter with Sub-mm w/ dDLR ( $1.3 \pm 0.5$  mm) ( $P = .001$ ) and Sub-mm w/o dDLR ( $1.4 \pm 0.4$  mm) ( $P = .017$ ) than with Standard ( $1.8 \pm 0.4$  mm) and was comparable between Sub-mm w/ and w/o dDLR ( $P = 1.000$ ) (Figure 5).

All the coronary segments could be qualitatively assessed except only 1 hypoplastic

segment (#3) in the single subject. In total, the subjective vessel sharpness was significantly better with Sub-mm w/ dDLR ( $3.9 \pm 0.3$ ) than Sub-mm w/o dDLR ( $2.4 \pm 0.7$ ) and Standard ( $2.5 \pm 0.7$ ) ( $P < .001$ , for both) and was comparable between Sub-mm w/o dDLR and Standard ( $P = .569$ ) (Figures 6a and 7). The subjective vessel signal homogeneity was significantly improved from Sub-mm w/o dDLR ( $2.1 \pm 0.5$ ) to Standard ( $2.7 \pm 0.6$ ) to Sub-mm w/ dDLR ( $3.9 \pm 0.3$ ) ( $P < .001$ , for all) (Figures 6b and 7). Even if divided into the proximal, middle, and distal coronary segments, the similar results

regarding the sharpness and signal homogeneity were obtained (Figure 6a and b). Particularly, both the sharpness and signal homogeneity were graded 3 or 4 in all the segments with Sub-mm w/ dDLR, whereas the sharpness was graded uninterpretable in 9 segments (11%) by reader 1 and 8 segments (10%) by reader 2, and the signal homogeneity was graded uninterpretable in 4 segments (5%) by Readers 1 and 2 with Standard. Inter-reader agreement was excellent ( $\kappa = 0.84$ ).

WHCMRA using Sub-mm w/ dDLR well delineated all 3 vessels, even in the distal segments, as shown in Figure 8.

## Discussion

The diameter in the proximal segments of the major coronary vessels is typically 2-4 mm and is smaller in the distal segments. Thus, WHCMRA is commonly limited in the delineation of distal coronary segments and the quantification of vessel lumen stenosis due to its insufficient spatial resolution and anisotropy. The state-of-the-art 3-T MR scanner with the high gradient magnetic field used in the present study can offer thinner slice images without increasing sampling interval or time in clinical settings. The latest dDLR based on DCNN using soft shrinkage as an activation function has been introduced using our MR scanner in order to reduce image noise.<sup>11</sup> The soft shrinkage aims to provide noise level adaptive denoising with a single CNN without the need to train a unique CNN for each noise level.<sup>11</sup> Unlike some smoothing filter designed to reduce high-frequency noise at the cost of image blurring, dDLR was confirmed to only reduce image noise on coronary vessel delineation. Its potential application to different frameworks may be valuable when combined with image acquisition acceleration techniques.<sup>14</sup> With adequate setting of the targeted noise level, the quality of dDLR may be improved to further reduce image noise, improve image quality, and reduce acquisition time in WHCMRA.

As our study results, both the SNR and CNR were significantly greater and both the subjective vessel sharpness and signal homogeneity were significantly better in noncontrast WHCMRA with Sub-mm w/ dDLR than with Sub-mm w/o dDLR. Thus, use of the dDLR was beneficial for not only reducing image noise but also improving definition of the vessel border in WHCMRA.

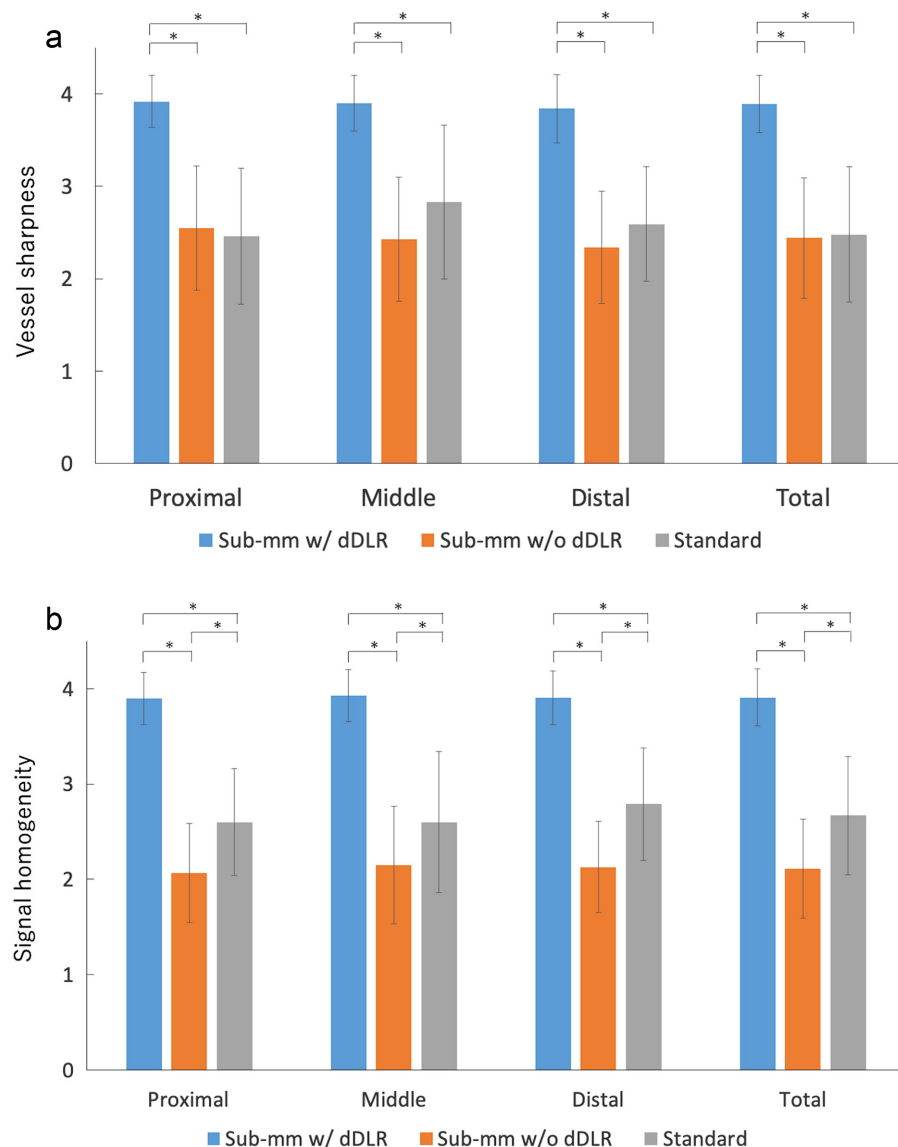


**Figure 6.** Bar graphs representing subjective image quality scores regarding vessel sharpness (a) and signal homogeneity (b) for the proximal, middle, distal, and all coronary segments in WHCMRA with Sub-mm w/ (blue) and w/o dDLR (orange) and Standard (gray). For the proximal, middle, distal, and all coronary segments, the subjective vessel sharpness (a) is significantly better with Sub-mm w/ dDLR than Sub-mm w/o dDLR and Standard ( $P < .001$ , for both) and is comparable between Sub-mm w/o dDLR and Standard ( $P > .05$ ). The subjective vessel signal homogeneity (b) is significantly improved from Sub-mm w/o dDLR to Standard to Sub-mm w/ dDLR ( $P < .001$ , for all). The asterisks represent statistical significance ( $P < .05$ ).

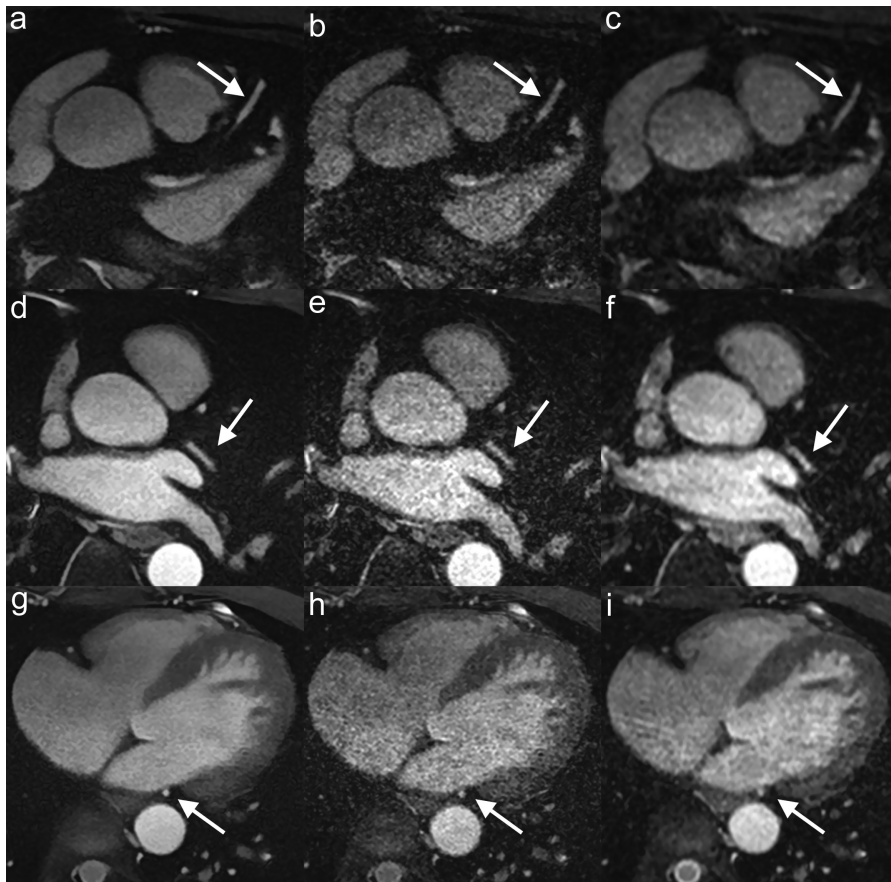


**Figure 7.** Axial images of WHCMRA showing #8 (arrow) for 50- (a-c), #11 (arrow) for 57- (d-f), and #13 (arrow) for 54-year-old men (g-i) with Sub-mm w/ (a, d, g) and w/o dDLR (b, e, h) and Standard (c, f, i). For the first subject (a-c), subjective image quality scores regarding vessel sharpness with Sub-mm w/ (a) and w/o dDLR (b) and Standard (c) were 4, 3, and 3 by both the readers, respectively, and those regarding signal homogeneity, 4, 2, and 3. For the second subject (d-f), subjective image quality scores regarding vessel sharpness with Sub-mm w/ (d) and w/o dDLR (e) and Standard (f) were 4, 2, and 3 by both the readers, respectively, and those regarding signal homogeneity, 4, 2, and 3. For the third subject (g-i), subjective image quality scores regarding vessel sharpness with Sub-mm w/ (g) and w/o dDLR (h) and Standard (i) were 4, 3, and 2 by both the readers, respectively and those regarding signal homogeneity, 4, 2, and 3.

On the other hand,  $ESRD_{20\%-80\%}$  was comparable between Sub-mm w/ and w/o dDLR, demonstrating no cost of image blurring by dDLR. While both the SNR and CNR were comparable,  $ESRD_{20\%-80\%}$  and the subjective

vessel sharpness and signal homogeneity were significantly improved with Sub-mm w/dDLR compared with Standard. These positive results regarding the subjective image quality by Sub-mm w/ dDLR were

similarly obtained in the proximal, middle, and distal coronary segments. Our 3-T MR scanner with the high gradient magnetic field in combination with dDLR successfully offered Sub-mm at the same bandwidth with preserving noise properties compared with Standard. Particularly, the subjective image quality was almost perfect with Sub-mm w/ dDLR, whereas image interpretability was occasionally limited with Standard. Usefulness of this combination of this MR scanner and dDLR has never been described to improve image quality and interpretability in WHCMRA with Sub-mm, whereas Yokota et al.<sup>12</sup> reported that dDLR significantly improved CNR of coronary arteries in high-resolution but non-Sub-mm WHCMRA (voxel size:  $1.8 \times 0.6 \times 1.0 \text{ mm}^3$ ) resulting in both higher visual image quality and better vessel traceability compared with standard-resolution WHCMRA (voxel size:  $1.8 \times 1.1 \times 1.7 \text{ mm}^3$ ) using the same MR scanner.

Because of the difference in the scan sequence, the acquisition time with Sub-mm was longer than that with Standard in the present study but was shorter than that with typical clinical protocols at 1.5 T.<sup>1,5,9</sup> The shorter acquisition time has the potential to improve spatial resolution and reduce image artifacts caused by motion instability during the long acquisition time. We used parallel imaging and the wheel technique in Fast 3D mode but could further reduce the acquisition time by applying compressed sensing or other advanced techniques, in near future, with the assistance of an improved version of dDLR.<sup>4-6,10</sup>

The proposed study was limited because it included only a small number of healthy adult subjects from a single institution. We assessed image quality only in the major coronary vessels and not in their branches.

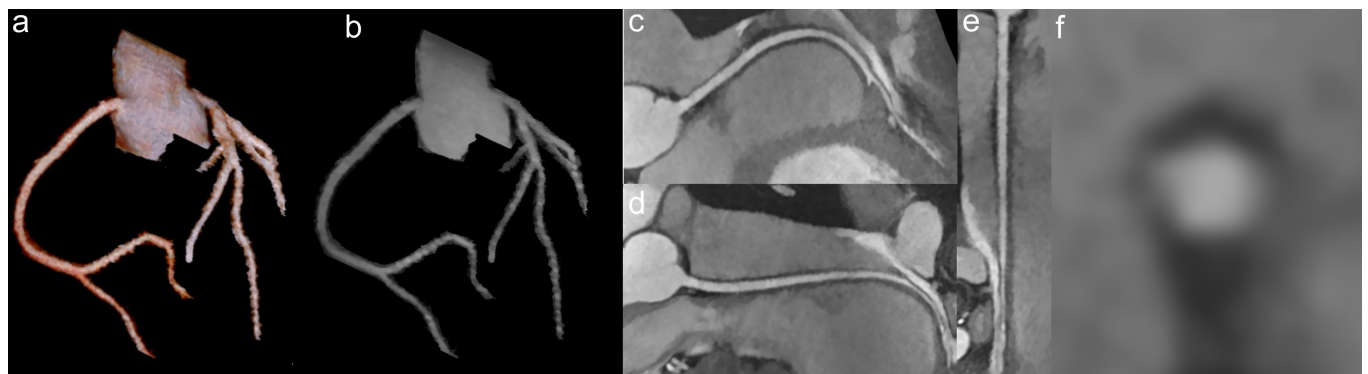


**Figure 8.** Data for a 37-year-old man. (a) Volume-rendered, (b) maximum intensity projection, and (c and d) curved MPR WHCMRA for RCA and (e) its stretched and (f) short-axis views using Sub-mm with dDLR, which show excellent delineation of all the major coronary vessels with little image noise, even in the distal segments. MPR, multiplanar reformation; RCA, right coronary artery.

Further studies of the clinical usefulness of noncontrast WHCMRA using Sub-mm w/dDLR are needed in order to improve diagnostic accuracy in a larger cohort with coronary artery disease at multiple institutions. The navigator gating efficiency of most patient populations is approximately 30%-50%, which is lower than that of a healthy cohort, and this leads to a longer acquisition time.<sup>4</sup> The voxel size in the standard WHMRA may be slightly larger than that in most clinical protocols (range: 1.1-1.3 mm).<sup>1,2,5</sup> Because we used parallel imaging, the noise quantification might depend on the g-factor maps and thus differ across the field of view. Our findings may also have been influenced by the smaller body physique of our Japanese volunteers, as compared to that of average-sized patients in Western countries.

In conclusion, application of dDLR is useful for reducing image noise and improving vessel sharpness, signal homogeneity, and delineation of the coronary arteries and thus image interpretability in noncontrast WHCMRA of Sub-mm compared with Standard WHCMRA using the 3-T MR scanner with the highest gradient magnetic field.

#### Acknowledgments

The authors are grateful to Mr. Kensuke Shinoda, Shuhei Takemoto, and Hiroshi Kusahara from MRI Systems Division, Canon Medical Systems Corporation for supporting this study.

#### Conflict of interest disclosure

The authors declared no conflicts of interest.

#### References

1. Sakuma H, Ichikawa Y, Chino S, Hirano T, Makino K, Takeda K. Detection of coronary artery stenosis with whole-heart coronary magnetic resonance angiography. *J Am Coll Cardiol.* 2006;48(10):1946-1950. [\[CrossRef\]](#)
2. Kato S, Kitagawa K, Ishida N, et al. Assessment of coronary artery disease using magnetic resonance coronary angiography: a national multicenter trial. *J Am Coll Cardiol.* 2010;56(12):983-991. [\[CrossRef\]](#)
3. Yoon YE, Kitagawa K, Kato S, et al. Prognostic value of coronary magnetic resonance angiography for prediction of cardiac events in patients with suspected coronary artery disease. *J Am Coll Cardiol.* 2012;60(22):2316-2322. [\[CrossRef\]](#)
4. Akçakaya M, Basha TA, Chan RH, Manning WJ, Nezafat R. Accelerated isotropic sub-millimeter whole-heart coronary MRI: compressed sensing versus parallel imaging. *Magn Reson Med.* 2014;71(2):815-822. [\[CrossRef\]](#)
5. Addy NO, Ingle RR, Wu HH, Hu BS, Nishimura DG. High-resolution variable-density 3D cones coronary MRA. *Magn Reson Med.* 2015;74(3):614-621. [\[CrossRef\]](#)
6. Bustin A, Ginami G, Cruz G, et al. Five-minute whole-heart coronary MRA with sub-millimeter isotropic resolution, 100% respiratory scan efficiency, and 3D-PROST reconstruction. *Magn Reson Med.* 2019;81(1):102-115. [\[CrossRef\]](#)
7. Stuber M, Botnar RM, Fischer SE, et al. Preliminary report on in vivo coronary MRA at 3 Tesla in humans. *Magn Reson Med.* 2002;48(3):425-429. [\[CrossRef\]](#)
8. Nezafat R, Stuber M, Ouwerkerk R, Gharib AM, Desai MY, Pettigrew RI. B1-insensitive T2 preparation for improved coronary magnetic resonance angiography at 3 T. *Magn Reson Med.* 2006;55(4):858-864. [\[CrossRef\]](#)
9. Liu X, Bi X, Huang J, Jerecic R, Carr J, Li D. Contrast-enhanced whole-heart coronary magnetic resonance angiography at 3.0T: comparison with steady-state free precession technique at 1.5T. *Invest Radiol.* 2008;43(9):663-668. [\[CrossRef\]](#)
10. Nakamura M, Kido T, Kido T, et al. Non-contrast compressed sensing whole-heart coronary magnetic resonance angiography at 3T: A comparison with conventional imaging. *Eur J Radiol.* 2018;104:43-48. [\[CrossRef\]](#)
11. Kidoh M, Shinoda K, Kitajima M, et al. Deep learning based noise reduction for Brain MR imaging: tests on phantoms and healthy volunteers. *Magn Reson Med Sci.* 2020;19(3):195-206. [\[CrossRef\]](#)
12. Yokota Y, Takeda C, Kidoh M, et al. Effects of deep learning reconstruction technique in high-resolution non-contrast magnetic resonance coronary angiography at a 3-Tesla machine. *Can Assoc Radiol J.* 2021;72(1):120-127. [\[CrossRef\]](#)
13. Uetani H, Nakaura T, Kitajima M, et al. A preliminary study of deep learning-based reconstruction specialized for denoising in high-frequency domain: usefulness in high-resolution three-dimensional magnetic resonance cisternography of the cerebellopontine angle. *Neuroradiology.* 2020. [\[CrossRef\]](#)
14. Kato Y, Ambale-Venkatesh B, Kassai Y, et al. Non-contrast coronary magnetic resonance angiography: current frontiers and future horizons. *Magma.* 2020;33(5):591-612. [\[CrossRef\]](#)
15. Taguchi S, Tambo M, Watanabe M, et al. Prospective validation of vesical imaging-reporting and data system using a next-generation magnetic resonance imaging scanner—is denoising deep learning reconstruction useful? *J Urol.* 2020. [\[CrossRef\]](#)
16. Ueda T, Ohno Y, Yamamoto K, et al. Compressed sensing and deep learning reconstruction for women's pelvic MRI denoising: utility for improving image quality and examination time in routine clinical practice. *Eur J Radiol.* 2021;134:109430. [\[CrossRef\]](#)
17. Suzuki S, Machida H, Tanaka I, Fukui R, Ueno E. Diameter measurement of vascular model on CT angiography using model-based iterative reconstruction: effect of tube current on accuracy. *AJR Am J Roentgenol.* 2014;202(2):437-442. [\[CrossRef\]](#)